

Emergent interactions lead to collective frustration in robotic matter

Onurcan Bektas^{1,2,†}, Adolfo Alsina^{2,3,†}, Steffen Rulands^{1,2*}

¹*Ludwig-Maximilians-Universität München,
Arnold-Sommerfeld-Center for Theoretical Physics,
Theresienstr. 37, 80333 München, Germany.*

²*Max-Planck-Institute for the Physics of Complex Systems,
Noethnitzer Str. 38, 01187 Dresden, Germany.*

³*GISC, Universidad Rey Juan Carlos,
Tulipán, 28933, Móstoles, Spain.*

[†] *These authors contributed equally.*

Current artificial intelligence systems show near-human-level capabilities when deployed in isolation. Systems of a few collaborating intelligent agents are being engineered to perform tasks collectively. This raises the question of whether robotic matter, where many learning and intelligent agents interact, shows emergence of collective behaviour. And if so, which kind of phenomena would such systems exhibit? Here, we study a paradigmatic model for robotic matter: a stochastic many-particle system in which each particle is endowed with a deep neural network that predicts its transitions based on the particles' environments. For a one-dimensional model, we show that robotic matter exhibits complex emergent phenomena, including transitions between long-lived learning regimes, the emergence of particle species, and frustration. We also find a density-dependent phase transition with signatures of criticality. Using active matter theory, we show that this phase transition is a consequence of self-organisation mediated by emergent inter-particle interactions. Our simple model captures key features of more complex forms of robotic systems.

The recent advances in artificial intelligence have brought about systems with near-human-level capabilities in some specific tasks. These advances mostly rely on deep neural networks, which can be trained efficiently using large data sets. In robotics, artificial intelligence is used to give robots the capability to interpret and manipulate their environment [1]. Recently, artificial intelligence systems are being combined to achieve better performance compared to individual systems [2–6]. In the context of robotics, such collectives contain multiple robotic units that are programmable and interact with their environment. Programmed interactions enable such robot collectives to create different formations [7–9] and react to global signals to manipulate objects [10].

Robot collectives have been experimentally implemented across spatial scales and system sizes [11, 12]. Due to the limitations imposed by miniaturization, there is a trade-off between the number of robots in a collective and the capacity of artificial intelligence that can be implemented in individual units. Macroscopic robot collectives comprise, for example, small groups of interacting robots which are each controlled by a performant artificial intelligence [13]. Smaller-scale robots are controlled by microcontrollers and can interact with thousands of robots for self-assembly, collective transport, collective perception, and more [7]. At the micron scale, robots interact via physical or chemical interactions between particles that are either self-driven active particles or particles driven by external forces and controlled via global signals. Such systems have, for example, been implemented as magnetic micro-disks driven by time-varying

magnetic fields. Due to their small scale, the capabilities of individual particles in these systems are limited and they are therefore usually controlled externally using global signals.

Conceptually, one can distinguish between different levels on which learning and execution occurs. In decentralised learning and decentralised execution, units learn and behave independently of each other [14]. In the case of centralised learning and decentralised execution, units are controlled by a single machine-learning algorithm, which has been employed in active matter systems to learn chemotactic behaviour [15, 16]. Finally, in the case of centralised learning and decentralised execution, where a single neural network is used by all particles individually but trained using the trajectory of all particles, 2D and 3D active intelligent swimmers moving collectively to reduce their energy expenditure [17]. Empirical studies in robot collectives have highlighted the emergence of subgroups of robots that may fulfil specialized tasks [18]. Such speciation phenomena include the emergence of implicit leaders that provide direction of guidance to other robots. Such experiments have also highlight the emergence of deadlock states, robots perform suboptimal behaviour [19–21].

Here, we study a paradigmatic theoretical framework for robotic matter that predicts key phenomena of empirical robot collectives. Specifically, we study stochastic many-particle systems in which each particle individually is endowed with artificial intelligence. In these systems the stochastic state transitions are defined by deep neural networks associated with each particle. The predictions by distinct deep neural networks are based on a particle's environment and they learn by analysing the particle's trajectory over time. We find that these systems ex-

* rulands@lmu.de

hibit complex spatio-temporal behaviour: Over time, increasingly complex interactions between particles evolve in a succession of temporal learning regimes. We observe the evolution of multiple particle species and frustration, where the system is locked long-term in a suboptimal state. We also find a density-dependent phase transition with signatures of criticality. Using active matter theory, we show that this phase transition exhibits signatures of criticality and is a consequence of self-organisation mediated by emergent interactions between particles.

RESULTS

Model definition

To begin, we consider a stochastic many-particle system where each particle, indexed by i , is described by a random variable, x_i , Fig. 1(a). The state of the system at a given time is then defined by the states of all N particles, $\{x_i\}_{i=1,\dots,N}$. The states of particles are updated according to transition rates between two states

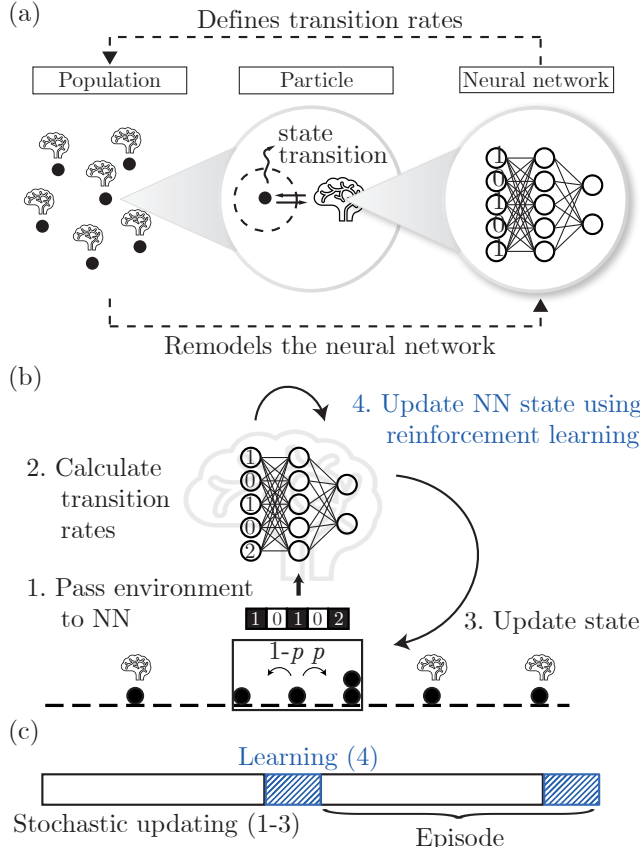


FIG. 1. Figure 1. (a) Feedback between collective particle dynamics and the evolution of deep neural networks in stochastic many-particle systems driven by deep learning. (b) One-dimensional lattice gas implementation. (c) Numerical protocol of stochastic updating and learning.

$\{x_i\}_{i=1,\dots,N}$ and $\{x'_i\}_{i=1,\dots,N}$ per unit time. These transition rates follow from the probabilities of each particle performing individual state transitions $x_i \rightarrow x'_i$. In our model, each particle is endowed with a unique deep neural network (DNN) which takes the system configuration, $\{x_i\}_{i=1,\dots,N}$, as an input and computes the single-particle transition rate as an output. Because the system configuration includes the states of other particles, the DNNs may encode effective interactions between particles. DNNs can, in theory, approximate any continuous functions up to any desired accuracy [22], such that the single-particle transition rates may, in principle, encode arbitrarily complex interactions. These interactions may change over time as particles learn from observing their past trajectories and update the parameters of their DNNs based on a reward function. Taken together, the particles in our model are endowed with sensors, processors and actuators [11]. The model describes a multi-scale system, in which DNNs determine the dynamics of individual particles and, vice versa, collective states on the macroscopic scale influence the learning of the parameters of DNNs. This gives two-way feedback between collective states emerging from effective interactions between particles on the macroscopic scale and the dynamics of DNN parameters, Fig. 1(a).

Here, to investigate the range of possible phenomenologies such systems may exhibit, we study the arguably simplest possible implementation of this framework. In this implementation, the state x_i of particles is defined by their position on a one-dimensional lattice of L sites with periodic boundary conditions, Fig. 1(b). A given particle i can hop to the right neighbouring site with probability p_i and to the left neighbouring site with probability $1 - p_i$. This fixes the unit of time. These transition rates are determined by the output layer of feed-forward DNNs which take the lattice environment of size l centered around a given particle as an input. The DNN parameters associated with a given particle are dynamically updated using deep reinforcement learning on the particles' past trajectory to maximise a discounted reward. The reward function gives a large negative reward when a particle moves to an already-occupied lattice site, and a small positive reward otherwise (Appendix A).

We used the kinetic Monte Carlo method to perform stochastic simulations of this model [23]. To reduce the computational cost of training the DNNs, we divided the simulation time into intervals, termed episodes, Fig. 1(c). During each episode, we updated the positions of particles while keeping the DNN parameters fixed. At the end of each episode, we updated the values of the DNN parameters using reinforcement learning. There are different algorithms for training a collection of agents: Multi-agent reinforcement learning (MARL) is used when multiple agents are in a common environment and should learn to cooperate or compete with each other [24–28]. Group-agent reinforcement learning (GARL) is used for cases in which each agent operates in a separate environment and only communicates with others to share knowl-

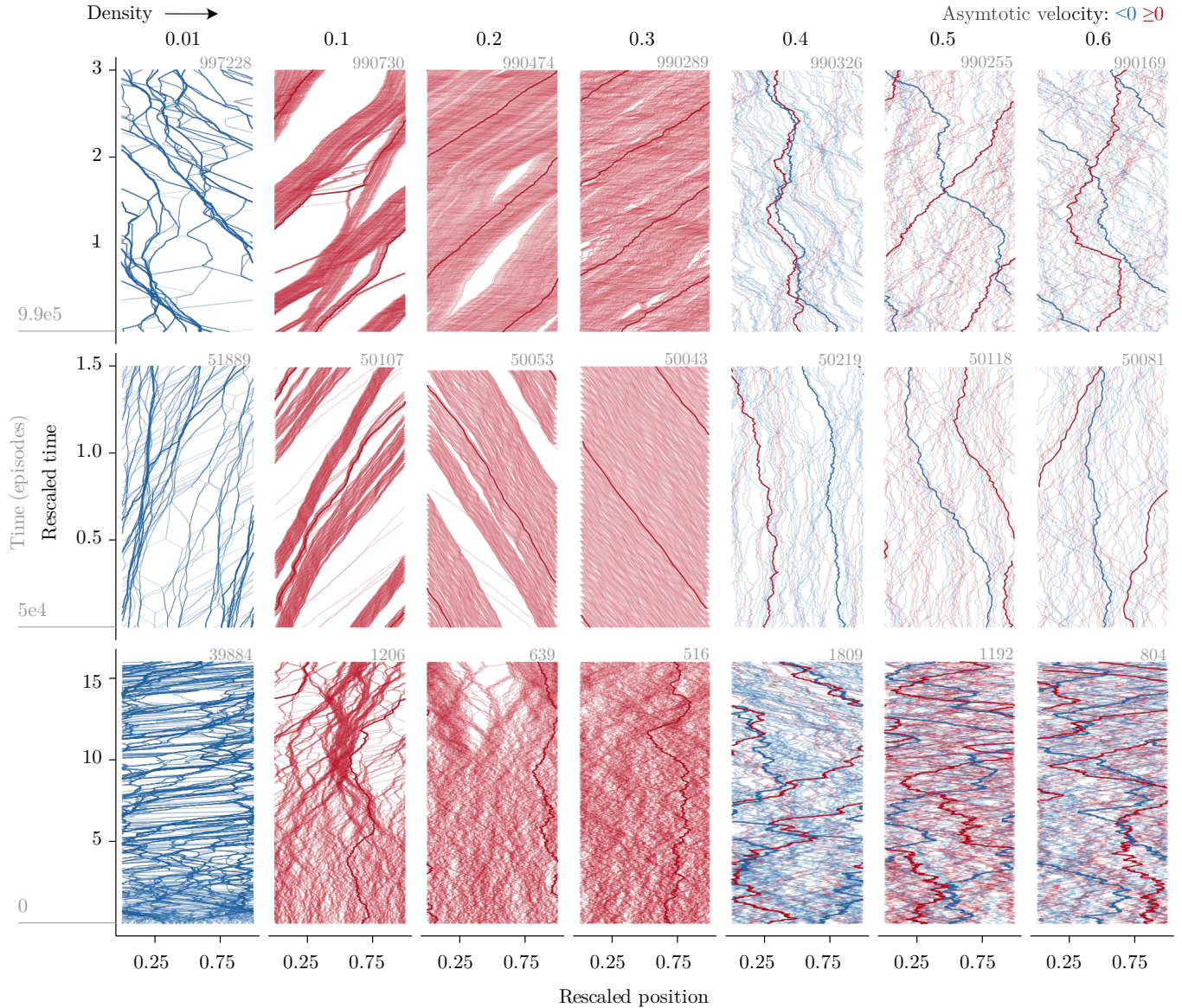


FIG. 2. Representative trajectories showing the positions of particles over time in distinct temporal regimes (rows). Each column corresponds to a simulation at the specified particle density. For visual purposes we rescaled positions and time in the following way: The x-axis is the lattice position divided by the total lattice size (from left to right $2\text{e}4$, $2\text{e}3$, $1\text{e}3$, $5\text{e}2$, $4\text{e}2$, 334 sites, respectively). The y-axis denotes the time in episodes divided by the typical time it takes for a particle to cross the system once. The starting time for each row is indicated in grey and the final time is on the top-right corner of each panel. Line colors show the sign of the average relative velocity of that particle in the last $2\text{e}5$ episodes of the simulations. Trajectories of representative particles are highlighted in bold. For densities 0.4, 0.5, and 0.6 we have randomly sampled 100 particles to make individual lines distinguishable.

edge [29, 30]. Here, we used an actor-critic reinforcement learning scheme with temporal-difference learning scheme to update the DNN parameters by maximising the cumulative discounted reward calculated from the particle trajectories in each episode [31] (see Methods). All figures shown here were obtained from simulations, where the number of particles, N , was set to 200, the local environment size, l , was 21, the system size, L , was set depending on particle density, and the discount factor, γ , was 0.9. DNNs had a triangular architecture with

21 neurons in the input layers, and 10, 5, and 2 neurons in the successive layers, respectively. We simulated up to $5 \cdot 10^6$ episodes with learning rate $5 \cdot 10^{-4}$. We also tested DNNs with up to five layers, but we observed no qualitative differences in the simulations. To simulate dilute systems without reducing the number of particles, we increased the number of lattice sites to achieve a given particle density while keeping the size of the environment, l , fixed. This was to ensure that the DNN sizes and the training dynamics at different particle densities

are consistent. This fixes the units of length to the lattice spacing.

From the definition of the model, several questions must be asked that in this form do not arise in active matter systems: First, particles appear in other particles' environment. Does this lead to the emergence of effective interactions between particles? If so, then, secondly, deep neural networks can, in principle, represent arbitrarily complex interactions that might be qualitatively different for each environment and each particle. Are robotic matter systems amenable to physics-type descriptions? Finally, would effective interactions between particles lead to collective behaviour as in other non-equilibrium systems studied in physics?

Dynamical regimes and density-dependent behaviour

Figure 2(a) shows representative trajectories of simulation results for different particle densities and different time windows in a given simulation. Despite the simplicity of the model, we find that particles form complex spatio-temporal structures after a short transient time. These structures change qualitatively over time, indicating that the dynamics transits through different temporal regimes. The spatio-temporal structures also depend on the particle density in that particles at low densities tend to align their velocity in the same direction, while above a density threshold of 0.3 particles at high densities move in opposite directions. In the following, we will analyse these changes as a function of the density more rigorously.

To this end, we first consider the relative velocity of particles with respect to each other. It is defined by the difference between the individual, instantaneous velocity of a given particle, v_i , and the average velocity in the system at a given time, $\langle v_i \rangle$, $v_i - \langle v_i \rangle$. We calculated the relative velocity for each particle and averaged over particles with the same sign of the asymptotic velocity. Figure 3(a) shows that, for low densities, the particles have vanishing relative velocities and therefore are moving in the same direction with a similar absolute velocity. Figure 3(b) shows that this occurs at a characteristic time $t_1 \approx 1e4$ episodes. For densities larger than 0.3, particles form two groups moving in opposite directions. This could reflect a random assignment of the direction of movement of particles. However, the variance of particles moving in a given direction across all simulations is smaller than what is expected from a statistically independent assignment and predicted by the binomial for millions of episodes ($p = 0.003$, F-test, Fig. 3(c)). Significantly, this implies that, in the high-density regime, the direction of particles is not chosen randomly, but tuned into a precisely balanced proportion of left- and right-moving particles on the system level.

The fine-tuning of particle directions to a 50-50 split at high densities seems counterintuitive given that they are

rewarded for not colliding with other particles. Indeed, while the average reward at low concentrations increases monotonically and reaches an optimal value, at high densities the reward first increases and then decreases at a time that is comparable to the formation of the two groups of particles, Fig. 3(d).

This observation raises two questions: first, what is the reason for the abrupt change in the behaviour of particles? And secondly, why is the high-density regime fine-tuned to a suboptimal reward? A potential answer to these questions could either be that particles learn different behaviours at high and low densities. This should then be reflected in the dynamics of the parameters of the DNNs. An alternative explanation could be that the abrupt change in behaviour emerges from self-organisation due to interactions between particles. In the following, we will aim to understand the origin of this behaviour by investigating in detail the spatio-temporal structures, the time evolution of neural networks, and emergent interactions between particles.

Spatio-temporal structures

To quantify the time evolution of spatial correlations between particle positions, we calculated the average distance to the nearest-neighbour particle over time, Fig. 4(a). In both density regimes, the nearest-neighbour distance decreases initially with time, showing that particles tend to cluster with other particles. The time evolution of the average nearest-neighbour distance is highly non-monotonic, reflecting different temporal regimes. Despite the formation of clusters, particles nevertheless reduce the probability of overlapping with other particles, Fig. 4(b). To further understand the time evolution of spatial structures we calculated the pair correlation function, which gives the average density of particles as a function of the distance to a given particle, Fig. 4(c). It shows that particles indeed cluster, but the sites adjacent to a given particle tend to be unoccupied. The pair-correlation function also shows that particle-particle correlations are longer in range in the low-density regime compared to the high-density regime.

Time evolution of neural network parameters

To test whether the formation of spatio-temporal structures and the change of particle behaviour with the density is correlated to patterns in the time evolution of the DNNs, we calculated probability density functions of the parameters defining the output of DNNs, namely the weights and biases, over time. Initialised with a Gaussian distribution, the distributions of DNN parameters develop different degrees of multi-modality over time, reflecting that DNN parameters converge to defined values, Fig. 5(a). The modality of the distributions of DNN parameters changes at the characteristic times defining

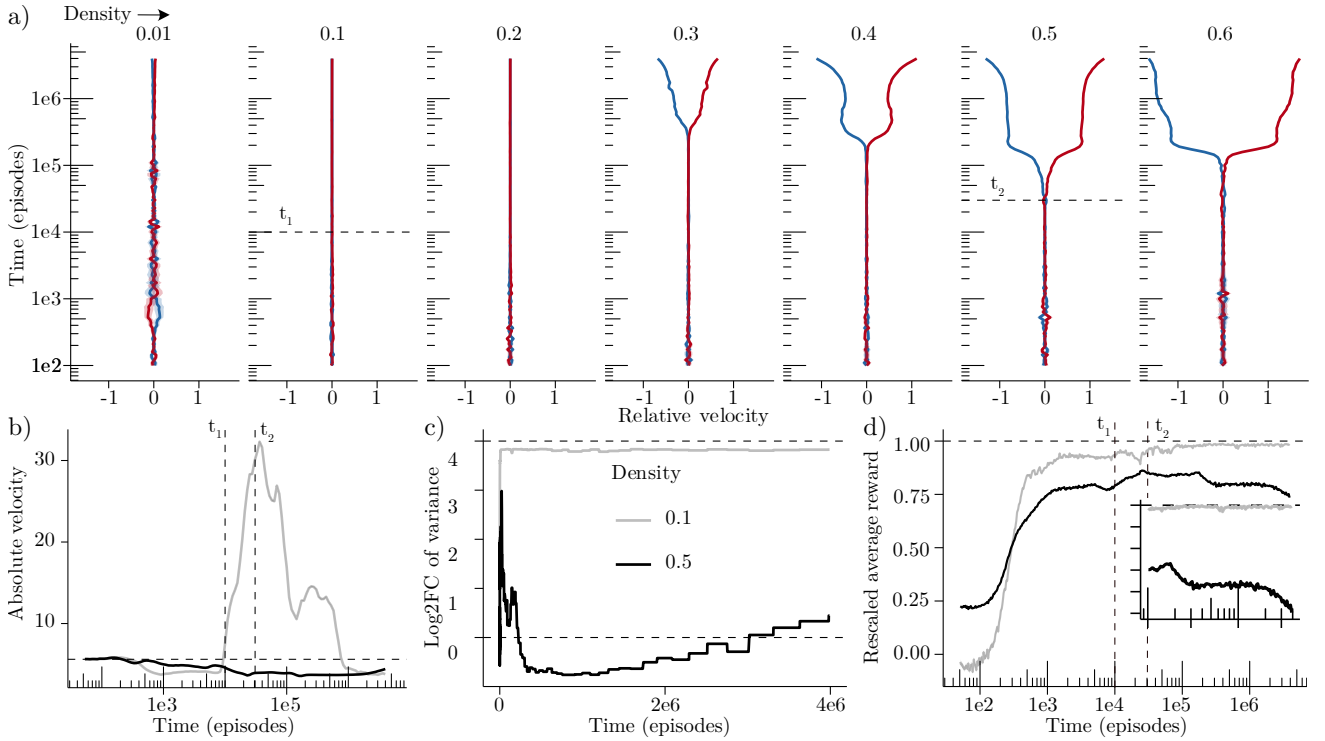


FIG. 3. (a) Average velocity of particles relative to the average velocity of all particles in a simulation. Particles are grouped by their asymptotic velocity, which is calculated as an average over the final 2e5 episodes of the simulations. The dashed lines on the time axis denote in this and in all following figure two characteristic times: $t_1 \approx 1e4$ episodes marks the initial formation of global alignment at low densities; $t_2 \approx 3e4$ episodes marks the initial formation of two groups of particles moving in opposite direction at high densities. (b) Average absolute velocity of all particles for two representative densities (colours defined in (c)). (c) Log2-fold change of the standard deviation of the number of right-moving particles across simulations. The lower horizontal dashed line is the variance expected if the direction of movement was assigned by chance. The upper dashed line is the maximal variance expected for globally aligned motion. (d) Average reward for two representative densities as a function of time. The inlay is a magnification that shows a decrease in the reward for density 0.5. Colours as in (c).

changes in the spatio-temporal behaviour, cf. Figs. 3 and 4. This suggests the existence of different learning regimes, where particles learn different input-output relations.

Analysis of interactions

To understand how the dynamics of the DNN parameters relate to the formation of spatio-temporal structures, we analyse the forces the DNNs encode. Intuitively, interactions between particles are encoded in the temporal change in its velocity, averaged over all environments. To develop this idea, we first represent a given environment by a vector \vec{e} , which contains the number of particles at each position in the environment. We now quantify the change in the velocity due to changes in the particle's environment. To this end, we note that the change in the velocity can be written as the product of changes due to changing environments, and the temporal evolution of the distribution of finding a given environment. Interactions are encoded in the former part, which is given by the directional gradient of the velocity with respect

to changes in the environment. In our case, the velocity is determined by the probability of hopping right in a given environment via $2p(\vec{e}) - 1$. Therefore, the directional derivative of the DNN output for a given input is a natural choice for quantifying interactions. To implement this, for a given environment \vec{e}_0 , we quantified the change in the transition rates p_i when the environment \vec{e}_0 is changed slightly by $\Delta\vec{e}$. Here, we perturb the environment $\Delta\vec{e}$ by the addition of a single particle. With this, we can quantify interactions by calculating the difference in the neural network output between the original environment and the perturbed environment,

$$\frac{p_i(\vec{e}_0 + \Delta\vec{e}) - p_i(\vec{e}_0)}{|\Delta\vec{e}|}. \quad (1)$$

To quantify the type of interactions more qualitatively, we multiply (1) with the sign of the distance of the particle in $\Delta\vec{e}$ to obtain a quantity that quantifies the degree with which particles are repulsed by the addition of a new particle to their environment (*repulsiveness*), $R = -\text{sign}(\Delta x) [p_i(\vec{e}_0 + \Delta\vec{e}) - p_i(\vec{e}_0)] / |\Delta\vec{e}|$. Negative values of the repulsiveness indicate attractive interactions.

To quantify the so-defined interactions for each par-

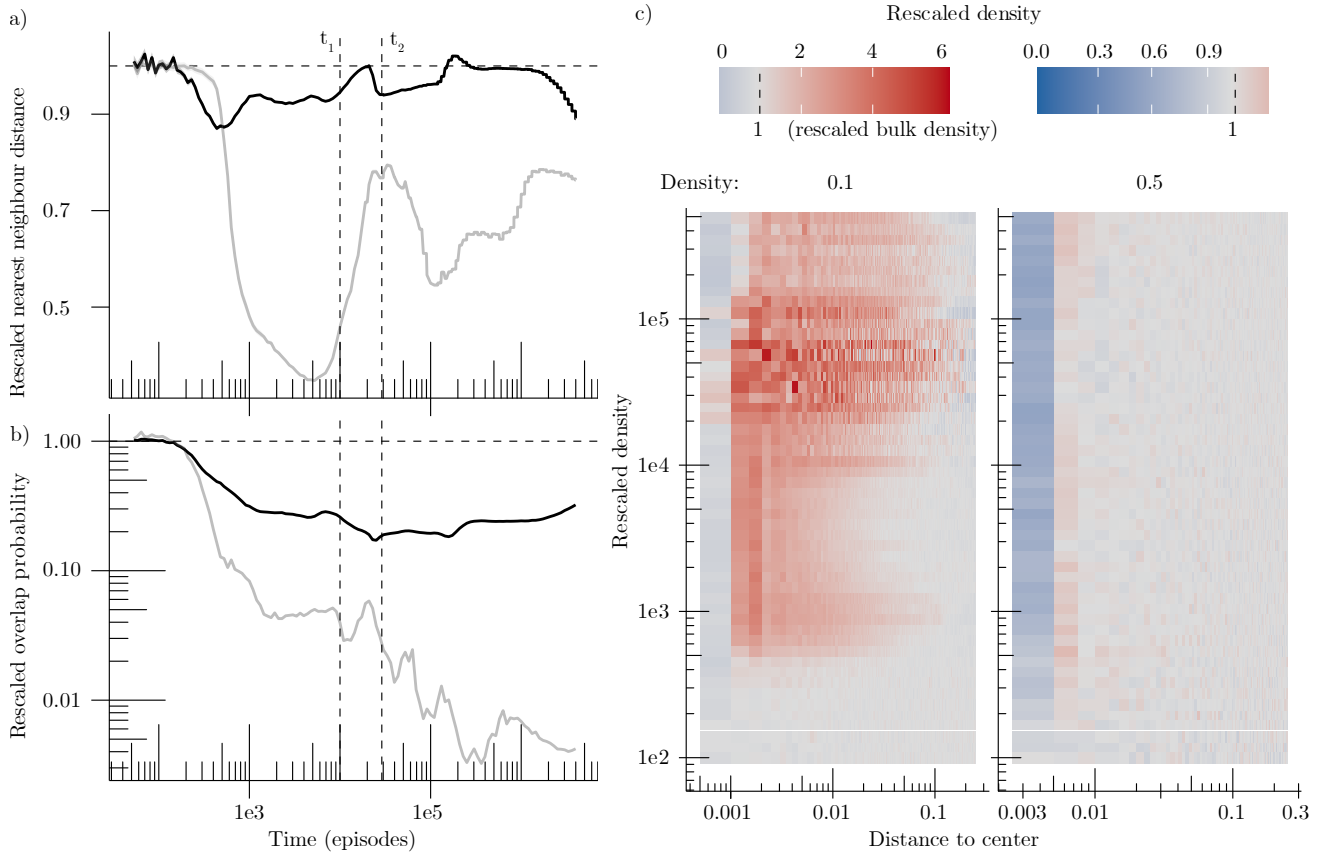


FIG. 4. (a) Average distance to the nearest-neighbour particle rescaled by the nearest-neighbour distance (NND) expected for a spatially uniform distribution of particles (horizontal dashed line). Vertical dashed lines denote characteristic times defined in Fig. 3. (b) Fraction of particles sharing a lattice site with at least one other particle rescaled by the expected value for a uniform distribution (horizontal dashed line). (c) Heatmaps of the pair correlation function for low and high particle densities. The pair correlation function is rescaled by the average density of particles (grey).

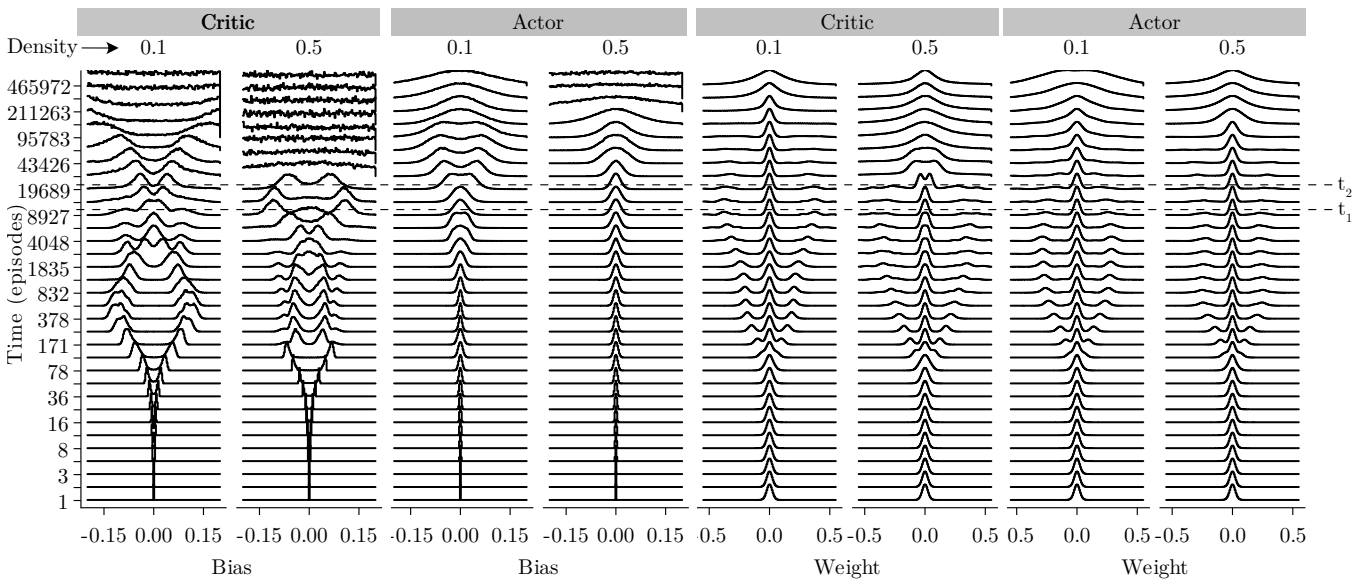


FIG. 5. Probability density functions of neural network parameters (black lines) for logarithmically spaced time points. Density functions are shown separately for two different densities, the actor and critic networks constituting the deep reinforcement learning algorithm and the weights and biases in the neural networks.

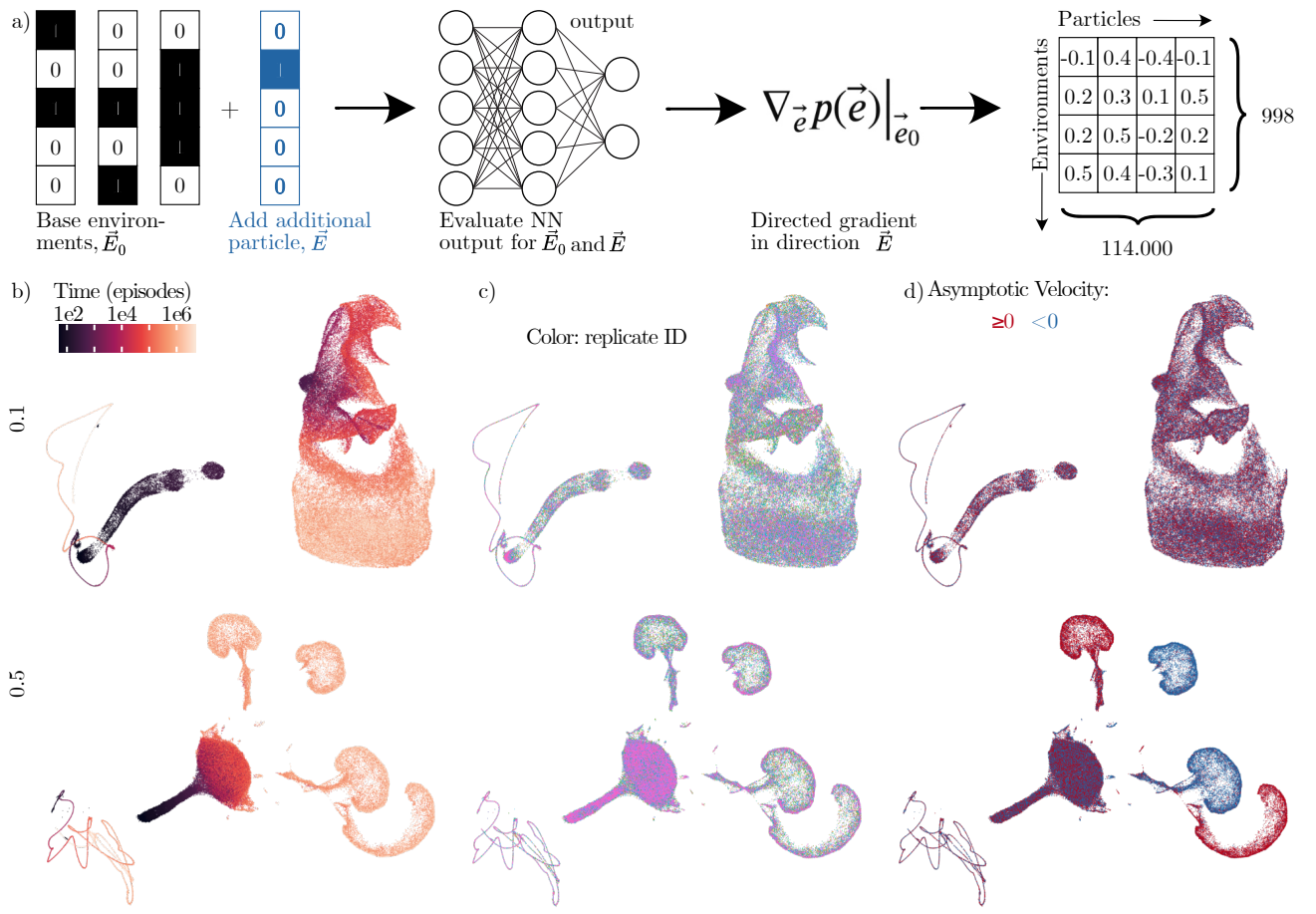


FIG. 6. (a) Schematic showing the computation of interactions. (b) Dimensionally reduced representations of interactions (UMAPs) for two representative densities (top and bottom). Each point represents one particle at a given simulation time and simulation run. Points that are close in the UMAP representation behave similarly in interactions. Colours signify simulation time, (c) simulation index, and (d) asymptotic velocity calculated in the final 2e5 episodes of the simulations.

ticle, we sampled 1000 random environments from the set of environments that host at most 6 particles. We passed these environments, and the corresponding environments that have one additional particle, to the DNNs of each particle at multiple time points, record the DNNs' output, and calculate the value of R , Fig. 6(a). Applying this procedure to all 1000 randomly-chosen environments, particles, and time points over 50 replicates per density leads to data with roughly 10^7 dimensions. As a first step towards quantifying interactions between particles, we therefore used a nonlinear dimensionality-reduction technique, uniform manifold approximation, and projection (UMAP), to obtain a first insight into the time evolution of interactions. Particles that are close in these projections tend to behave similarly in interactions. The UMAPs show the systematic time evolution of the response of particles to changes in their environments, Fig. 6(b). This time evolution is qualitatively different in the high and low density regimes, meaning that particles develop different interactions in both regimes, Fig. 6(b). All structures in the UMAPs are independent of the simulation run, Fig. 6(c), showing that particles consistently develop similar possible interactions across runs.

At high densities, we observe the emergence of four clusters of particles in the projected space after a time $2 \cdot 10^5$ which corresponds to the formation of the two groups of particles moving in different directions, Fig. 2(c). This means that particles evolve into four distinct species, which are distinguished by the way they interact with their environments. Two pairs of these clusters identify particles moving ballistically in a given direction, Fig. 6(c). Particles moving in the same direction further separate into two groups, which interact in different ways depending on higher-order properties of the environments. We were not able to identify simple rules that distinguish between interactions of particles in the clusters corresponding to particles moving in the same direction, showing that particles develop complex interactions that do not follow patterns as in other systems studied in statistical physics.

To gain deeper insights into these interactions, we parametrised environments by the distance of the particle in e_j , Δx , and the distance of the first and second nearest neighbours in \vec{e}_0 , k_1 and k_2 , respectively. Figure 7(a) shows that interactions are predominantly repulsive with a tendency for their strength to increase over time. This is expected by the choice of the reward function. Additionally, interactions tend to become longer in range over time, as particles obtain non-zero repulsion with respect to other particles at increasing distances. While particles at high densities only interact with the nearest and next-nearest neighbour sites particles at low densities interact over longer distances at large times. Figure 7(a) also shows characteristic branching points, that mark time points after which the response of particles in a given set of environments becomes non-homogeneous. At these time points, particles learn to distinguish an increasing number of different environments.

To investigate how interactions depend on the base environment \vec{e}_0 we further parametrised the base environment by the distance to the first nearest neighbour, k_1 , and the distance to the second nearest neighbor, k_2 . At low densities, particles first distinguish between base environments, where $k_1 = 1$ and k_2 is either equal or larger than 2, Figure 7(b). For low densities, after the emergence of nearest-neighbour repulsion, particles first learn to respond to the presence of a particle at a neighbouring site ($\Delta x = 1$) depending on the position of the second nearest-neighbour particle. Specifically, particles learn to distinguish between environments, where the second nearest neighbour is two sites away compared to a longer distance. Later, particles learn to respond to the presence of a particle two sites away ($\Delta x = 2$) depending on the position of a second nearest neighbour at the same distance. For high densities, after the emergence of nearest-neighbour repulsion, we observe a similar sequence of branching points but at later time points during the simulation.

A large number of environments tend to follow similar trends, indicating that the DNNs in particles do not distinguish between these environments in terms of repulsiveness and that DNNs initially do not interpret the full complexity of the environment. At characteristic times that partially overlap with the boundaries of the temporal regimes defined on the macroscopic scale we observe branching points after which environments become distinguishable by the DNNs to increasing degrees. Therefore, over time, DNNs of particles learn to distinguish between an increasing number of environments at characteristic time points. In between these time points, the form of interactions tends to be stable over increasingly long time periods.

Phenomenological theory

With this, we are now in a position to come back to the question of what is the origin of the abrupt change in the behaviour of particle as a function of the particle density and the associated decrease of rewards. Our analyses have shown both: macroscopic order in space and time, which indicates collective behaviour of particles; and highly complex, density-dependent interactions that depend on evolving particle “species”. To test the hypothesis that the abrupt change in the behaviour of particles is a consequence of self-organization, we now develop a minimal, phenomenological model that only comprises a minimal set of interactions without explicit density dependence.

To this end, we use the framework of active matter theory, and Langevin equations. We consider the position $x_i(t)$, and velocity $v_i(t)$ of a particle i at a given instance of time, t . The time evolution of the position and velocity of this particle is then described by a set of

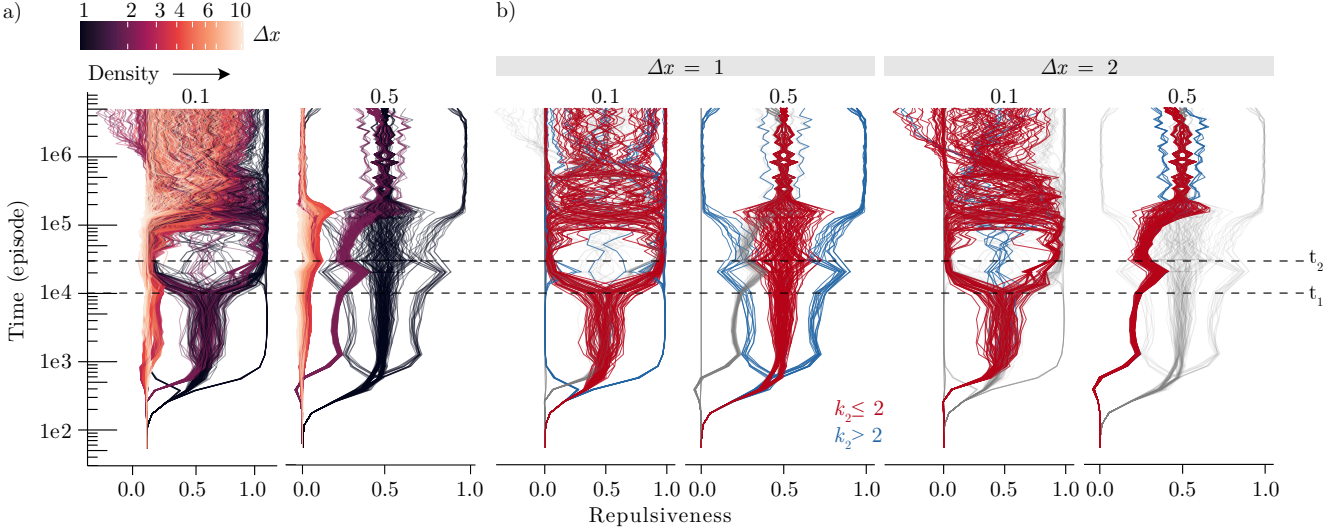


FIG. 7. To understand how interactions involve over time, we computed the time evolution of the repulsiveness, averaged over all particles. Each line shows the repulsiveness in a different environment. (a) Repulsiveness colored by the distance to the particle added to the base environments. (b) Repulsiveness for the case that a particle is added at a distance $\Delta x = 1$ to the base environments. Environments are coloured by the distance to the second nearest neighbour. (c) Repulsiveness for the case that a particle is added at distance $\Delta x = 2$ to the base environments. Environments are coloured by the distance to the second nearest neighbour.

Langevin equations of the form

$$\dot{x}_i = v_i, \quad (2)$$

$$\dot{v}_i = -\gamma(v_i)v_i + K_i + \sqrt{2D}\eta_i. \quad (3)$$

where $\gamma(v)$ is a generalized, non-equilibrium friction, K_i is the force acting between particle i and all other particles in its environment, D is the noise amplitude, and η is Gaussian white noise.

We first identify the shape of the interactions K_i from our simulations. To this end, we take a coarse-grained perspective and quantify the force acting on a particle i for a given average velocity field $u(x)$ and density field $\rho(x)$ averaged in a small environment around the position x_i , $K_i(\rho, u)$. In our simulations, interactions evolve over time and are highly complex. They cannot be easily translated into simple interaction rules. For the purpose of our argument, we identify two density-, particle, and species-independent components of interactions: First, we have shown in Fig. 7(b) that interactions between particles are predominantly repulsive. This gives rise to a contribution to the interaction term of the form $-\partial\rho(x)/\partial x|_{x=x_i}$.

Further, interactions aim to minimise not only the rate of collisions, but also their correlations. This is because particles maximise a discounted reward of the form $G = \sum_j \gamma^j r_j$ that depends not only on the instantaneous rate of collisions, but also on how they are correlated over time. Specifically, the expected discounted reward, $\langle G \rangle$ increases if the correlations in collisions decrease (Appendix D),

$$\langle G \rangle \sim -\tau_- \langle \rho \rangle (1 - \langle \rho \rangle) (1 - r_-) + \mathcal{O}(\tau_-^2), \quad (4)$$

where τ_- and τ_+ are the autocorrelation times of collisions and non-collisions, respectively. The minimisation of the autocorrelation time is empirically supported by our simulations (Fig. S1). The autocorrelation time is proportional to the time a pair of particles spend in each other's vicinity, such that particles minimise a function that is proportional to $1/|v-u|$. This then leads to a force that is given by the derivative of this term with respect to v , $\text{sign}(v-u)/|v-u|^2$. Because the correlation scales with the density, the second contribution to the interaction terms takes the form $\rho \text{sign}(v-u)/|v-u|^2$. Taken together, in our phenomenological description, this gives an effective force term for particle i of the form

$$K_i = \zeta \rho \frac{\text{sign}(v-u)}{|v-u|^2} - \delta \frac{\partial \rho}{\partial x} \Big|_{x=x_i}. \quad (5)$$

We now define the active friction term $\gamma(v)$. Because our system is out of equilibrium, the fluctuation-dissipation theorem does not hold, such that friction is not coupled to the noise amplitude. Instead, this term comprises a part that describes directed motion and a part that describes friction. A phenomenological term that describes both is the Rayleigh-Helmholtz friction [32], which has been used to describe a variety of active matter systems. It is of the form

$$\gamma(v) = -\alpha v + \beta v^3. \quad (6)$$

Taken together, in non-dimensional form, the time-

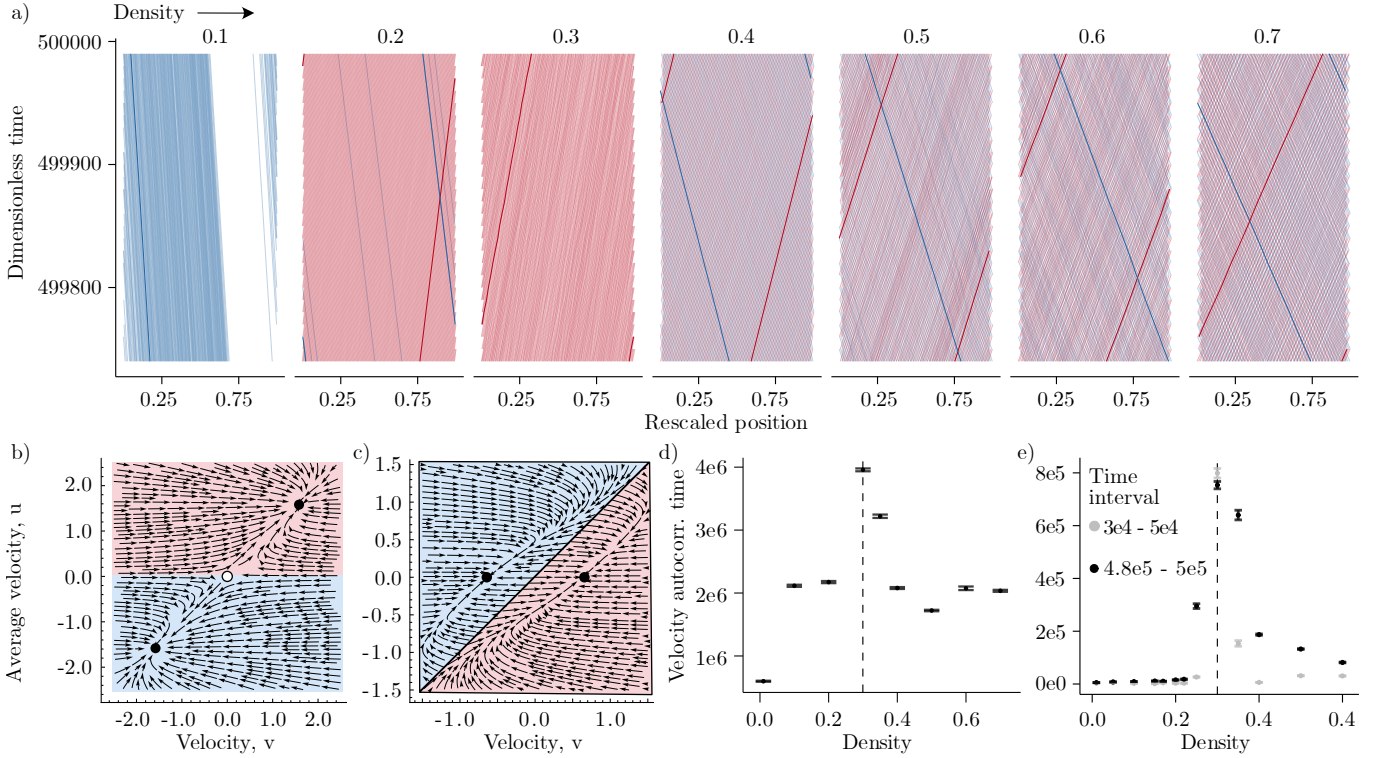


FIG. 8. a) Representative trajectories showing the positions of particles at the specified particle density in the last 200 episodes. The colors show the sign of average velocity of the particles in the last $1e3$ time points: red for positive and blue for a negative average velocity. b) Phase portrait of Eqs. (9) and (10) for density 0.1. c) phase portrait of Eqs. (9) and (10) for density 0.5. The colors show the sign of the velocity of the test particle in the Hartree approximation. d) velocity autocorrelation time obtained from simulations of Eqs. (7) and (8). The dashed line shows the density 0.3. e) Velocity autocorrelation time obtained from simulation of the full model in Fig. 1(b).

evolution of velocity and position of a given particle reads

$$\dot{x} = v, \quad (7)$$

$$\dot{v} = v - v^3 + s \frac{\rho \operatorname{sign}(v - u)}{(v - u)^2} - r \frac{\partial \rho}{\partial x} + \sqrt{B} \eta, \quad (8)$$

where we have dropped the index i . We have non-dimensionalised the Langevin equations by rescaling time and space by $t' = \alpha t$ and $x' = x\sqrt{\alpha\beta}$, respectively, and removed the apostrophes to simplify the notation. The dimensionless parameters $s = \zeta\sqrt{\beta^5/\alpha^3}$ and $r = \delta\sqrt{\beta^3/\alpha}$ quantify the strength of interactions due to the minimisation of correlations and repulsion relative to the effect of self-propulsion, respectively. $B = D\beta/\alpha^2$ is the dimensionless noise strength.

In this model, the relative strength of the two interaction terms implicitly depends on the particle density. For high densities, fluctuations in the particle density are weak, such that we expect the term that minimises correlations to dominate. Intuitively, this leads to a maximisation of the difference between the particle's velocity v and the average velocity u , which could globally lead to a split as observed in our simulations. For low densities, the term that minimises correlations is negligible and we expect particle repulsion to be dominant.

To test this numerically, we performed stochastic simulations of Eqs. (7) and (8) using a finite difference method (see Appendix C). We indeed found that particles show global alignment at low densities and a split into groups moving in opposite direction for high densities (Fig. 8). Again, the variance of particles moving in the positive direction across simulations is smaller than expected by chance ($p = 2.22e^{-16}$), suggesting a collective tuning of the sizes of both groups. These observations suggest that the abrupt change in the behavior of particles in Fig. 3(a) is a phase transition resulting from collective behavior induced by interactions between particles.

To investigate this more quantitatively, we analytically derived the coevolution of the velocity of a particle, v , and the average velocity of all particles \bar{u} . To this end, followed Ref. [33] and used a moment expansion up to second order in the average velocity to obtain a set of nonlinear differential equations,

$$\dot{v} = (1 - v^2)v + s \frac{\rho \operatorname{sign}(v - \bar{u})}{(v - \bar{u})^2} + r(\bar{u} - v), \quad (9)$$

$$\dot{\bar{u}} = \bar{u} - \bar{u}(\bar{u}^2 + 3T). \quad (10)$$

Here, $T = \langle (v - \bar{u})^2 \rangle$ is the variance of the velocities, which we estimated from our simulations of the Langevin

equations. The co-evolution of the velocity of individual particles and the average velocity is summarized in phase portraits (Fig. 8). The phase portraits show attractors that correspond to asymptotic dynamical regimes of Eqs. (7) and (8). For low densities, we find two attractors with $v = \bar{u}$ that correspond to states, where the velocity of particles aligns with the average velocity in the system. For high densities, these attractors are located horizontally on a line given by $\bar{u} = 0$. Therefore, the phenomenological model predicts the evolution of individual velocities to take specific positive or negative values under the constraint of a vanishing global velocity. Because the line $\bar{u} = 0$ is stable, fluctuations around it are suppressed by feedback mechanisms. This corresponds to the observed state with precisely tuned equal proportions of particles moving in either direction.

Taken together, our analysis shows that the abrupt change of the behaviour as a function of the particle density is an emergent phenomenon resulting from interactions between particles. It is therefore a phase transition as in statistical physics systems. For high densities, interactions between particles have the macroscopic effect. In this regime, particles optimise their reward locally, without being able to predict the suboptimal consequences of their behaviour on the macroscopic scale. This resembles a learning analogon to frustration phenomena in disordered systems or the fallacy of the commons in social sciences. This analysis raises the question of whether this phase transition resembles known phase transitions in (non-equilibrium) statistical physics. To investigate this, we calculated autocorrelation functions of the velocities of individual particles using the batch means method [34], both in the Langevin simulations and in the simulations of the full model comprising intelligent agents, for different particle densities. In both cases, the autocorrelation time diverges at the density at which the phase transition occurs. Diverging correlations are characteristic of critical points, suggesting critical behaviour. A further characterisation of the phase transition requires the computation of critical exponents, which is currently not feasible for intelligent agents. It is, however, of note that the phase transition occurs at a density, at which the range covered by the repulsive interactions of each particle multiplied by number of particles equals the lattice size, that is, the effective volume fraction is equal to 1. This could indicate a relation to jamming transitions.

DISCUSSION

Taken together, we studied a paradigmatic model of robotic matter. In this model, particles in a stochastic lattice gas are endowed with deep neural networks that take the spatial environment of a particle as an input and predict transition rates. Our extensive simulations reveal a rich phenomenology, including complex emergent phenomena leading to a phase transition, the evolution of multiple particle species, temporal learning regimes, and

a phenomenon akin to frustration, where particles adopt suboptimal strategies. The phase transition we observe shows signs of criticality. Although it is not possible to determine critical exponents, the behaviour close to the phase transition point shows similarities to a jamming transition.

Stochastic many-particle systems as the one studied in this work differ qualitatively from systems typically studied in active matter theory: because each particle has many more intrinsic degrees of freedom than the number of particles one can typically simulate on computers, they effectively lack microscopic symmetries. While in statistical physics one is typically interested in the breaking of microscopic symmetries, here the question arises if symmetries emerge as a consequence of learning, and whether these symmetries are then broken again. Because deep neural networks of sufficient size can, in principle, approximate arbitrarily complex function interactions between particles do not necessarily follow simple patterns. They may be qualitatively different between particles and environments. This raises the question of in how far physical theories are adequate in describing the time evolution of such systems. In our work, particles indeed developed complex interactions that cannot be described by simple mathematical functions. However, a simple phenomenological theory focussing on rudimentary aspects of these interactions is able to predict a key aspect of the system, namely the existence of a density-dependent phase transition.

Although our model is a drastic simplification of real robotic systems, our results show similarities to much more complex robotic systems. For example, Ref. [19] studied a hide and seek game between intelligent agents, in which agents passed through different, metastable learning regimes and interactions between agents lead to a decrease in the collected reward. Apart from interacting robots, also virtual artificial intelligence systems, like the widely-used large-language systems, are now beginning to be combined in order to achieve better performance [35]. This raises the question of how to design these systems to achieve an expected outcome. In some cases, interacting learning objectives straightforwardly translate into collective behaviour [14]. Our work implies that learning can be drastically influenced in unpredictable manners by collective behaviour on the macroscopic scale.

ACKNOWLEDGEMENTS

We thank Alexander Ziepke, Stefano Bo, Frank Jülicher, and the entire Rulands group for helpful discussions.

AUTHOR CONTRIBUTIONS

A.A. and O.B. contributed equally. A.A., O.B., and S.R. conceptualized the work. A.A. and S.R. supervised

the work; O.B. wrote the simulation code and analysed O.B. performed analytical calculations. S.R. acquired funding. O.B. and S.R. wrote the initial draft of the manuscript. All authors edited and approved of the final version of the manuscript.

[1] S. Russell and P. Norvig, Artificial Intelligence, Global Edition (2021).

[2] A. Mordvintsev, E. Randazzo, E. Niklasson, and M. Levin, Growing Neural Cellular Automata, *Distill* **5**, e23 (2020).

[3] E. Randazzo, A. Mordvintsev, E. Niklasson, M. Levin, and S. Greydanus, Self-classifying MNIST Digits, *Distill* **5**, e00027.002 (2020).

[4] D. Pathak, C. Lu, T. Darrell, P. Isola, and A. A. Efros, Learning to Control Self-Assembling Morphologies: A Study of Generalization via Modularity (2019).

[5] Y. Tang and D. Ha, The Sensory Neuron as a Transformer: Permutation-Invariant Neural Networks for Reinforcement Learning (2021).

[6] M. J. Matarić, From Local Interactions to Collective Intelligence, in *Prerational Intelligence: Adaptive Behavior and Intelligent Systems Without Symbols and Logic, Volume 1, Volume 2 Prerational Intelligence: Interdisciplinary Perspectives on the Behavior of Natural and Artificial Systems, Volume 3*, edited by H. Cruse, J. Dean, and H. Ritter (Springer Netherlands, Dordrecht, 2000) pp. 988–998.

[7] M. Rubenstein, A. Cornejo, and R. Nagpal, Programmable self-assembly in a thousand-robot swarm, *Science* **345**, 795 (2014).

[8] J. Werfel, K. Petersen, and R. Nagpal, Designing Collective Behavior in a Termite-Inspired Robot Construction Team, *Science* **343**, 754 (2014).

[9] A. Becker, G. Habibi, J. Werfel, M. Rubenstein, and J. McLurkin, Massive uniform manipulation: Controlling large populations of simple robots with a common input signal, in *2013 IEEE/RSJ International Conference on Intelligent Robots and Systems* (2013) pp. 520–527.

[10] F. Arvin, A. E. Turgut, F. Bazyari, K. B. Arikhan, N. Bel-lotto, and S. Yue, Cue-based aggregation with a mobile robot swarm: A novel fuzzy-based method, *Adaptive Behavior* **22**, 189 (2014).

[11] H. Löwen and B. Liebchen, Towards Intelligent Active Particles (2025), arXiv:2501.08632 [cond-mat].

[12] V. A. Baulin, A. Giacometti, D. A. Fedosov, S. Ebbens, N. R. Varela-Rosales, N. Feliu, M. Chowdhury, M. Hu, R. Füchslin, M. Dijkstra, M. Mussel, R. Van Roij, D. Xie, V. Tzanov, M. Zu, S. Hidalgo-Caballero, Y. Yuan, L. Cocconi, C.-M. Ghim, C. Cottin-Bizonne, M. C. Miguel, M. J. Esplandiu, J. Simmchen, W. J. Parak, M. Werner, G. Gompper, and M. M. Hanczyc, Intelligent soft matter: Towards embodied intelligence, *Soft Matter* **21**, 4129 (2025).

[13] M. Hüttenrauch, A. Šošić, and G. Neumann, Deep Reinforcement Learning for Swarm Systems, *Journal of Machine Learning Research* **20**, 1 (2019).

[14] M. Durve, F. Peruani, and A. Celani, Learning to flock through reinforcement, *Physical Review E* **102**, 012601 (2020).

[15] S. Tovey, C. Lohrmann, and C. Holm, Emergence of chemotactic strategies with multi-agent reinforcement learning, *Machine Learning: Science and Technology* **5**, 035054 (2024).

[16] J. Grauer, F. Jan Schwarzenbach, H. Löwen, and B. Liebchen, Optimizing collective behavior of communicating active particles with machine learning, *Machine Learning: Science and Technology* **5**, 015014 (2024).

[17] S. Verma, G. Novati, and P. Koumoutsakos, Efficient collective swimming by harnessing vortices through deep reinforcement learning, *Proceedings of the National Academy of Sciences* **115**, 5849 (2018).

[18] I. Slavkov, D. Carrillo-Zapata, N. Carranza, X. Diego, F. Jansson, J. Kaandorp, S. Hauert, and J. Sharpe, Morphogenesis in robot swarms, *Science Robotics* **3**, eaau9178 (2018).

[19] B. Baker, I. Kanitscheider, T. Markov, Y. Wu, G. Powell, B. McGrew, and I. Mordatch, Emergent Tool Use From Multi-Agent Autocurricula (2020).

[20] M. Bettini, A. Shankar, and A. Prorok, Heterogeneous Multi-Robot Reinforcement Learning (2023).

[21] A. Reina, R. Zakir, G. De Masi, and E. Ferrante, Cross-inhibition leads to group consensus despite the presence of strongly opinionated minorities and asocial behaviour, *Communications Physics* **6**, 1 (2023).

[22] G. Cybenko, Approximation by superpositions of a sigmoidal function, *Mathematics of Control, Signals and Systems* **2**, 303 (1989).

[23] D. T. Gillespie, A general method for numerically simulating the stochastic time evolution of coupled chemical reactions, *Journal of Computational Physics* **22**, 403 (1976).

[24] S. V. Albrecht, F. Christianos, and L. Schäfer, *Multi-Agent Reinforcement Learning: Foundations and Modern Approaches* (MIT Press, 2024).

[25] R. Lowe, Y. Wu, A. Tamar, J. Harb, P. Abbeel, and I. Mordatch, Multi-Agent Actor-Critic for Mixed Cooperative-Competitive Environments (2020).

[26] B. Baker, I. Kanitscheider, T. Markov, Y. Wu, G. Powell, B. McGrew, and I. Mordatch, Emergent Tool Use From Multi-Agent Autocurricula (2020), arXiv:1909.07528.

[27] A. Lazaridou, A. Peysakhovich, and M. Baroni, Multi-Agent Cooperation and the Emergence of (Natural) Language (2017).

[28] E. A. Duñez-Guzmán, K. R. McKee, Y. Mao, B. Coppin, S. Chiappa, A. S. Vezhnevets, M. A. Bakker, Y. Bachrach, S. Sadedin, W. Isaac, K. Tuyls, and J. Z. Leibo, Statistical discrimination in learning agents (2021).

[29] K. Wu and X.-J. Zeng, Group-Agent Reinforcement Learning (2023) pp. 37–48.

[30] K. Wu, X.-J. Zeng, and T. Mu, Group-Agent Reinforcement Learning with Heterogeneous Agents (2025).

- [31] R. S. Sutton and A. G. Barto, *Reinforcement Learning: An Introduction*, second edition ed., Adaptive Computation and Machine Learning Series (The MIT Press, Cambridge, Massachusetts, 2018).
- [32] U. Erdmann, W. Ebeling, L. Schimansky-Geier, and F. Schweitzer, Brownian particles far from equilibrium, *The European Physical Journal B - Condensed Matter and Complex Systems* **15**, 105 (2000).
- [33] P. Romanczuk and U. Erdmann, Collective motion of active Brownian particles in one dimension, *The European Physical Journal Special Topics* **187**, 127 (2010).
- [34] M. B. Thompson, A Comparison of Methods for Computing Autocorrelation Time, arXiv (2010).
- [35] Grok 4 | xAI.

A. IMPLEMENTATION OF THE STOCHASTIC SIMULATIONS

We used the Gillespie algorithm to simulate the particle transitions [23]. We set the total propensity of each particle to 1, as a result, we draw a random number Δt , the time increment, from an exponential distribution with rate $50N$ where N is the total number of particles. This choice of time-increment allowed each particle to make 50 transitions on average in any given episode. We chose one particle randomly at each time increment. Then we allowed the chosen particle observe its current environment, feed it into its neural network, generate the transition probabilities from its neural network and transition to left or right using those transition rates. We defined the reward function such that, if the particle moves to an empty side, it earns a positive reward, $+1$, and otherwise a negative reward, -100 . We record the environments the particles observed, the actions they took, and the reward they got at every transition. After a time interval $\Delta t = 1$, we ended the episode any trained the neural networks of all particles using the triplet (observed environment, action taken, reward taken). To train the actor, in accordance with temporal-difference learning, we used the loss

$$\sum_{i=1}^{n_j-1} -A_i \log p_i,$$

where n_j is the number of transitions the particle j made during the episode, and $A_i := R_i + \gamma V_{i+1} - V_i$, and p_i, R_i, V_i are the probability with which the particle made the transition, the reward it got and the value predicted by the critic at step i , respectively. To train the critic, we used the loss $\sum_{i=1}^{n_j-1} A_i^2 / (n_j - 1)$.

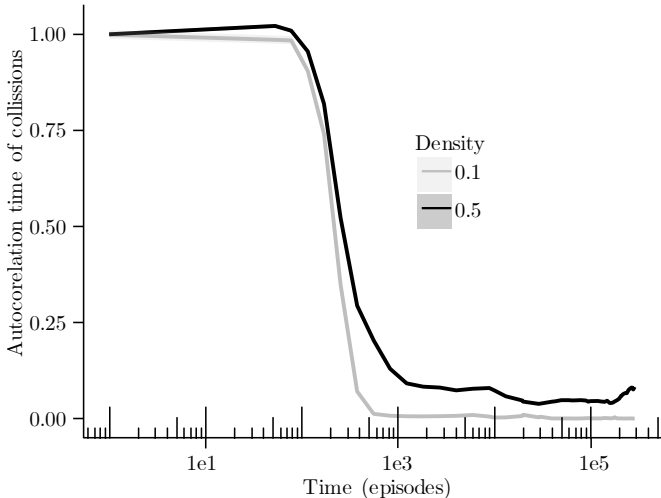


FIG. S1. The average autocorrelation time of collisions over 10 replicates. The shaded area around the curves denote the standard error. The averages are calculated at logarithmically samples time points.

B. NUMERICAL SOLUTION OF THE LANGEVIN EQUATIONS

We used the Euler scheme to integrate the Langevin equations. We used 200 particles with time increment $\delta t = 0.01$, and the system size was determined based on $L = 200/\langle \rho \rangle$ where $\langle \rho \rangle$ is the average particle density. We used periodic boundary conditions. We set $s = 1.17, r = 12.50, B = 0.02$, and we used a local radius of 5 to calculate the local density field $\rho(x)$ and the local velocity field $u(x)$ for each particle. We run 15 to 24 replicates per particle density. To calculate the gradients of the local fields, we subtracted value of the field in the right of the particle at distance 5 from the value of the field in the left of the particle at distance 5, and divided this by 5.

C. NON-DIMENSIONALISATION OF THE LANGEVIN EQUATION

To non-dimensionalize the Langevin equations, we rescaled time and positions as

$$t' := \alpha t$$

$$x' := \sqrt{\alpha\beta}x.$$

This leads to a rescaling of velocities as

$$v' := \sqrt{\frac{\beta}{\alpha}}v,$$

$$u' := \sqrt{\frac{\beta}{\alpha}}u,$$

and of the particle density as

$$\rho' := \frac{\rho}{\sqrt{\alpha\beta}}.$$

The rescaled noise term reads

$$\eta' := \frac{\eta}{\sqrt{\alpha}}.$$

Using these normalised variables, we obtain dimensionless Langevin equations of the form

$$\frac{dx'}{dt'} = v', \quad (S.1)$$

$$\frac{dv'}{dt'} = v' - v'^3 + \zeta \sqrt{\frac{\beta^5}{\alpha^3}} \frac{(\rho')^2 \operatorname{sign}(v' - u')}{(v' - u')^2} \quad (S.2)$$

$$- \delta \sqrt{\frac{\beta^3}{\alpha}} \partial_{x'} \rho' + \sqrt{\frac{2D\beta}{\alpha^2}} \eta'. \quad (S.3)$$

D. MINIMISATION OF THE AUTOCORRELATION TIME OF COLLISIONS INCREASES THE DISCOUNTED REWARD

In this appendix, we show that the expected discounted reward, $\langle G \rangle$, increases as autocorrelation time of the col-

lisions $\tau_- = \int_0^\infty \langle \delta(R_0 - r_-) \cdot \delta(R_t - r_-) \rangle dt$ decreases. First, remember that, we can express the expected discounted reward, $\langle G \rangle$, as a sum over the expected discounted reward conditioned on the reward observed at zero-th step, R_0 ,

$$\langle G \rangle = \sum_{r \in \{r_-, r_+\}} P(R_0 = r) \langle G | R_0 = r \rangle.$$

Suppose that the particles are randomly distributed across the system, then the probability of R_0 being r_- , namely the probability of collision, is given by the average particle density, $\langle \rho \rangle$, hence

$$\langle G \rangle = \langle \rho \rangle \langle G | R_0 = r_- \rangle + (1 - \langle \rho \rangle) \langle G | R_0 = r_+ \rangle. \quad (\text{S.4})$$

Notice that, by the definition of G , the conditional expectation, $\langle G | R_0 = r \rangle$, is,

$$\begin{aligned} \langle G | R_0 = r \rangle &= \int_0^\infty dt \gamma^t \langle R_t | R_0 = r \rangle \\ &= \int_0^\infty dt \gamma^t \left(\langle R_t \rangle + e^{-t/\tau} (r - \langle R_0 \rangle) \right), \end{aligned} \quad (\text{S.5})$$

where τ is the autocorrelation time of the reward of type r . Combining Eq. (S.4) and Eq. (S.5), and evaluating the integral, we obtain

$$\begin{aligned} \langle G | R_0 = r \rangle &= \frac{1}{\log(\gamma)} \left[\frac{\langle \rho \rangle (r_- (\langle \rho \rangle - \tau_- \log(\gamma)) - \langle \rho \rangle + 1)}{\tau_- \log(\gamma) - 1} - \frac{(\langle \rho \rangle - 1) (\langle \rho \rangle r_- - \tau_+ \log(\gamma) - \langle \rho \rangle + 1)}{\tau_+ \log(\gamma) - 1} \right] \\ &\sim C - \tau_- \langle \rho \rangle (1 - \langle \rho \rangle) (1 - r_-) + \mathcal{O}(\tau_-^2) \quad \text{as } \tau_- \rightarrow 0 \end{aligned} \quad (\text{S.6})$$

where we set r_+ to 1 in equation (S.6), and C is inde-

pendent of the autocorrelation time of collisions τ_- . As a result, decreasing τ_- will increase $\langle G \rangle$.